Influence of diffusion plane orientation on electrochemical properties of thin film LiCoO2 electrodes

Journal of The Electrochemical Society, **149** (6) A699-A709 (2002)
0013-4651/2002/149(6)/A699/11/$7.00 © The Electrochemical Society, Inc.

Influence of Diffusion Plane Orientation on Electrochemical Properties of Thin Film $LiCoO_2$ Electrodes

P. J. Bouwman,[a,*,z] B. A. Boukamp,[a,] H. J. M. Bouwmeester,[a] and P. H. L. Notten[b,c,**]**

[a]*Laboratory of Inorganic Materials Science, Faculty of Chemical Technology and MESA+ Research Institute, University of Twente, 7500 AE Enschede, The Netherlands*
[b]*Philips Research, 5656 AA Eindhoven, The Netherlands*
[c]*Eindhoven University of Technology, 5600 MB Eindhoven, The Netherlands*

Submicrometer $LiCoO_2$ films have been prepared on silicon substrates with RF sputtering and pulsed laser deposition (PLD). The electrochemical activity of both types of thin film electrodes is compared using scanning cyclic voltammetry, galvanostatic and potentiostatic intermittent titration, and electrochemical impedance spectroscopy. The RF films exhibit *a* axis orientation and have an accessible diffusion plane alignment, unlike the *c* axis oriented PLD films. The preferential orientation of the host crystal lattice toward the electrolyte solution is critical for the intercalation rate and cycling efficiency. The RF films show superior electrochemical performance and faster relaxation characteristics than the PLD films. Based on the analysis of the time and frequency domain measurements a model for the electrode response is proposed. Apparently, the intercalation rate of the RF films is not diffusion-limited, but hindered by the large charge-transfer resistance, the phase boundary movement, and the hindrance by the solid electrolyte interface.
 [DOI: 10.1149/1.1471543]

Manuscript submitted August 20, 2001; revised manuscript received December 11, 2001. Available electronically April 12, 2002.

The key to the rechargeable lithium battery is the reversible lithium intercalation mechanism. In the lithium-ion cell it exists in both the anode and cathode. The positive electrode of such a rocking chair cell consists of a transition metal oxide, the negative electrode usually has a carbonaceous composition. The power of the cell depends on the rate capability of the electrodes and, hence, the kinetics of the lithium intercalation. The exchange current of typical commercial LiC_6 and $LiCoO_2$ composite electrodes differ by approximately two orders of magnitude.[1] The positive $LiCoO_2$ electrode is expected to be rate-limiting during intercalation. The solid-state diffusion of lithium within the host intercalation structure is regarded as one of the slower processes involved.

The transition oxide materials can roughly be divided into rock-salt related and spinel structures, *e.g.*, $LiCoO_2$ and $LiMn_2O_4$, respectively. The first type is layered with lithium in octahedral sites between O-Co-O sheets. Hence, it exhibits two-dimensional pathways for lithium diffusion via neighboring vacancies.[2] The second type has a three-dimensional lithium network and allows stable lithium occupation of octahedral as well as tetrahedral sites, thus enabling 3D diffusion. In commercial composite powder electrodes the intercalation host grains are embedded in a porous carbon/binder mixture to allow maximum exposure toward the electrolyte solution. The characteristic diffusion length L is determined by the particle size distribution. For a randomly oriented polycrystalline thin film electrode a virtual 3D diffusion is obtained. Hence, the characteristic length, L, is of the order of the film thickness.

This contribution deals with submicrometer $LiCoO_2$ films, which can be prepared with contrasting preferential orientations. The polycrystalline film structure has been characterized in a previous publication.[3] The films deposited with RF sputtering (RF films) reveal a preferential (110) plane orientation, indicating that the diffusion planes are aligned vertically to the substrate surface, toward the electrolyte solution. Due to this favorable orientation a high intercalation rate is expected.[4] The films prepared with pulsed laser deposition (PLD films) reveal a preferential (00*l*) (*c* axis) orientation and have the diffusion planes parallel to the substrate surface. As a result of this adverse alignment the diffusion length L is large and the transport of lithium is expected to be slow.[5]

The electrode interface area and the exposure of the host lattice diffusion planes to the electrolyte solution are influenced by the film morphology. Using substrates with a large surface roughness results in nonuniform films containing irregularities, which are not necessarily detrimental for the intercalation process. Particularly PLD film properties have been observed to improve with the application of polished stainless steel[6-8] and aluminum sheet substrates,[9] due to significant surface roughness. To demonstrate the influence of the host lattice orientation on the intercalation behavior without interference of substrate morphology, only silicon wafer substrates are used for the RF and PLD films in this publication.

Experimental

Silicon wafers (110 orientation, n-type) served as substrate material for film deposition with PLD and RF sputtering. The wafer was laser cut into 15 mm ∅ disks. The rear and sides of these disks were covered with 200 nm aluminum using RF sputtering. This metallic film served as back-side contact for electrochemical measurements connecting the probe with the conducting silicon. Prior to the deposition of the $LiCoO_2$ an additional aluminum film (200 nm) was sputtered as current collector (optional) together with an adhesion layer of 50 Å titanium applied between the aluminum and the $LiCoO_2$ film. The $LiCoO_2$ films are grown on heated substrates (300°C) under a low oxygen background pressure (0.02 to 0.2 mbar). For the exact deposition parameters for PLD films as well as RF films we refer to published work.[3] All films discussed in this paper have been annealed at 550°C for 30 min. High temperature XRD was used to optimize the annealing procedure to produce highly oriented, polycrystalline films. The film composition was analyzed with inductively coupled plasma (ICP) emission spectroscopy.

The electrochemical analysis was performed using a PGstat20 Autolab Potentiostat (ECO-Chemie) with integrated frequency response analyser. The electrochemical cell is constructed from Kel-F, a polymer, which is highly resistant to organic electrolytes. The working electrode sample is glued in a rotating disk electrode (RDE) and positioned above the lithium counter electrode. Commercial battery grade liquid electrolyte [1 M $LiClO_4$, ethylene carbonate: diethyl carbonate (EC:DEC) 1:1, Merck] is used. In a three-electrode configuration a Luggin capillary containing a strip of metallic lithium, is used as reference electrode. The counter electrode is a piece of 2 × 2 cm lithium foil (thickness 1 mm) pressed onto the grooved surface of the nickel-plated copper (bottom) plate. This plate also seals the bottom of the electrolyte compartment. The top of the electrolyte compartment is closed off by a slip-ring envelop-

* Electronical Society Student Member.
** Electrochemical Society Active Member.
z E-mail:bouman@ct.utwente.nl

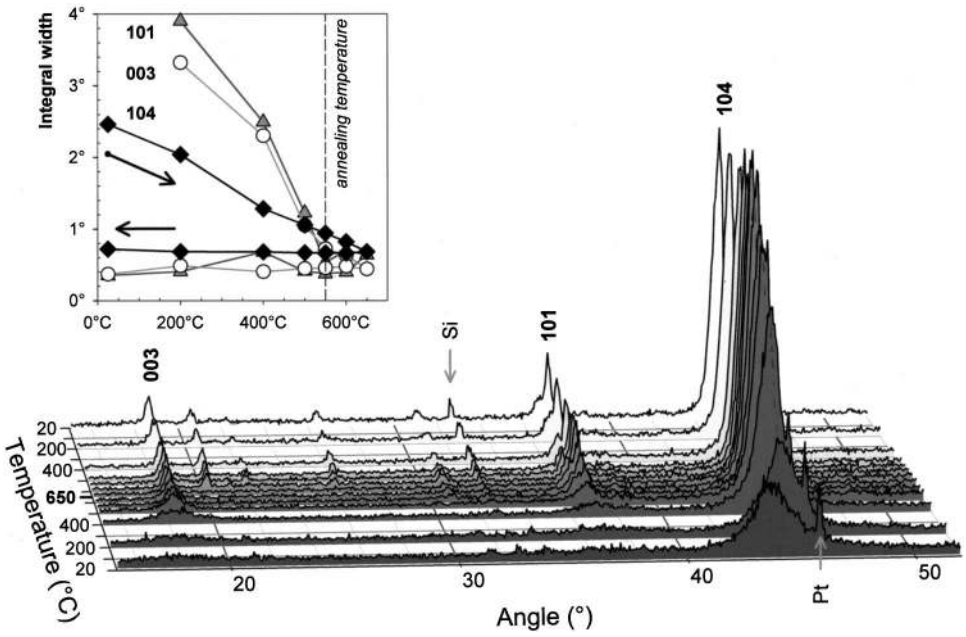

Figure 1. XRD spectra of an RF film exhibiting [104] preferential orientation, recorded *in situ* during annealing treatment up to 650°C and down to room temperature (ramp rate 2°C min^{-1}, mounted on Pt heating element). The inset shows the integral width of the main diffraction peaks as a function of temperature.

ing the RDE tip. This construction minimizes evaporation of the volatile organic solvents and thus reduces crystallization of the salt at the circumference. The cell is operated inside a helium glove box.

The copper bottom plate of the electrochemical cell also conducts heat produced or extracted by the two underlying 36 W Peltier elements. These devices allow accurate temperature control of the electrochemical cell. The temperature is recorded automatically with an AD590 linear temperature sensor, which is in contact with the electrolyte solution and connected to the data acquisition computer.

Results

Upon deposition of the RF and PLD films the preferential orientation of the polycrystalline $LiCoO_2$ film is directly perceptible from the specific broad diffraction peaks of the lattice planes aligned parallel to the substrate surface. Figure 1 shows the evolution of the crystal structure with annealing treatment, as measured with high temperature XRD on a preferential [104] RF film, for this purpose directly deposited on a silicon substrate. The inset shows a decrease of the integral width (=width of a fitted rectangle exhibiting equal height and area as the diffraction peak) of the major $LiCoO_2$ diffraction peaks. This integral width stabilizes above 550°C. Annealing treatment at higher temperatures or for long periods of time leads to lithium deficiency, formation of Co_3O_4, and other by-products and outgrowth of crystals, all of which are detrimental to the structural uniformity of the $LiCoO_2$ film.[3] The as-deposited films maintain their stoichiometric composition within the limit of accuracy of the analysis method (<3%) when the standard annealing procedure (550°C, 30 min) is used. After electrochemical cycling, excess oxygen is detected at the surface. Fourier transform infrared spectroscopy (FTIR) reveals strong C═O vibration absorbance and indicates the presence of carbonate compounds, most likely from decomposition of the electrolyte solvents.

A liquid electrolyte is chosen to guarantee good ionic contact between the electrodes and to enable the use of a rotating disk electrode (RDE) to study interface-related phenomena. No clear dependency of the electrochemical behavior of the thin film $LiCoO_2$ electrode on the rotation velocity is observed. Hence, in order to reduce noise the measurements have been performed with a stationary RDE.

Upon cell assembly the open circuit potential (OCP) *vs*. lithium varies with time between 3.0 and 3.5 V. After passing a small amount of charge (deintercalation) a stable OCP is obtained. Using slow scanning cyclic voltammetry (SSCV) the current is monitored, while the potential is increased with a rate of 0.1 mV s^{-1} to the first vertex potential of 4.2 V and subsequently decreased down to the second vertex potential of 3.3 V (3.5 V for the RF films). In Fig. 2 the first and second scan of an RF and a PLD $LiCoO_2$ electrode are shown. The first scan is irreproducible. In subsequent scans the electrochemical capacity and faradaic yield of the RF film are close to their theoretical values. The cathodic peak potential of the RF film is located at 3.72 V in the first scan and decreases slightly in the second scan. No distinct anodic peak is observed, even when the scan range was temporarily increased to 4.4 V. The PLD electrode exhibits low capacity and poor faradaic yield. At this scan rate only low currents are observed with no specific anodic or cathodic peaks, except for the small cathodic peak at 3.72 V in the first scan.

Figure 3a shows the actual potential response of a 0.75 μm RF film to multiple 200 s current pulses of 50 μA and Fig. 3b of a 0.2 μm PLD film to 400 s pulses of 2.5 μA. Each current pulse is followed by a period of zero current relaxation to allow the system to reach equilibrium before the next pulse is applied. The PLD film is charged with smaller current pulses to avoid excessive overpotentials and consequential electrolyte decomposition. Note that during the first charging pulses of the RF film the voltage drops as a result of a large decrease in overpotential with progressing lithium deintercalation.

The extent of potential relaxation of the RF film upon current termination is orders of magnitude smaller than that of the PLD film. The voltage at the end of the relaxation period (1 h and 3 h for the RF and PLD film, respectively) is assumed to represent the open circuit potential (OCP), although the potential of the PLD film still shows a gradual decay. These values are plotted in Fig. 4 for both types of films: the RF film OCP (◇) as function of x in Li_xCoO_2 on the bottom x axis and the PLD film OCP (■) as function of absolute capacity on the top axis. Note that the scale of the top axis is interrupted and stretched to show a similarity between both curve trends [capacity = 0.75 C corresponds to a fully deintercalated PLD film ($x = 0$)].

As the assumed OCP of the PLD film depends strongly on the chosen equilibration time, mutual comparison of the OCP curves is not realistic, unless mathematical correction is applied. The potential relaxation of both films can be described accurately with an empirical, double exponential function

$$E(t) = E^{eq} + a\exp(-t/\tau_a) + b\exp(-t/\tau_b) - \dot{E}^{decay}t \quad [1]$$

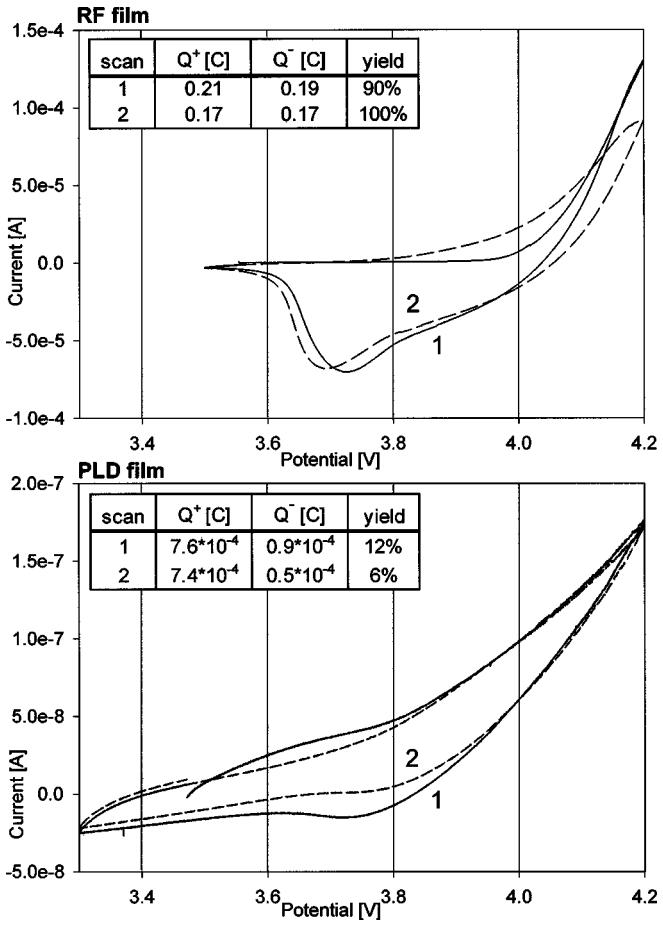

Figure 2. Cyclic voltammogram of a 0.75 μm RF film and a 0.2 μm PLD film recorded at 0.1 mV/s scan rate against metallic lithium plotted on different vertical scales. The charge introduced during oxidation (Q^+), extracted during reduction (Q^-), and the efficiency (%) of the first and second scan are noted in the inset table.

where E^{eq} is the new OCP potential, a and b the pre-exponential factors of the two inverse exponential functions with time constants τ_a and τ_b, respectively, and $\dot{E}^{decay}\ t$ the product of potential decay (assumed constant) and time. This last term represents the continuous self-discharge of the cell, while the other parameters characterize the potential relaxation process, stabilizing at E^{eq}. Typical sets of fit parameters are listed in Table I. The calculated E^{eq} values represent the true OCP(x), corrected for self-discharge. These values have also been plotted in Fig. 4 for the RF (◇) and the PLD film (□). For the RF film the correction is insignificant, while for the PLD film the discrepancy between the experimental and the corrected OCP is quite large.

Figure 5a shows the fit of an RF and PLD film potential relaxation curve to Eq. 1 and the relative deviation from the experimental data ($dV < 0.01\%$). The accuracy of the fit is limited by the bit noise of the measurement equipment. Both curves shown in Fig. 5a exhibit $E^{eq} = 3.99$ V. Here, the ratio between time constants τ_a and τ_b is commonly a factor of ten. Both τ values are slightly lower for the RF film. The dissimilarity in relaxation behavior of both films is mainly reflected by the tenfold difference in the pre-exponential factors. Note that the parameters enable mutual comparison, but have not yet been given physical interpretation.

The parameter $\dot{E}^{decay}$ is in fact $[d(OCP)/dt]$ in units [V s^{-1}] (for an open cell). This value can be translated into an apparent leakage current defined in amperes by correcting for the voltage intercalation profile using the calculated parameter E^{eq}

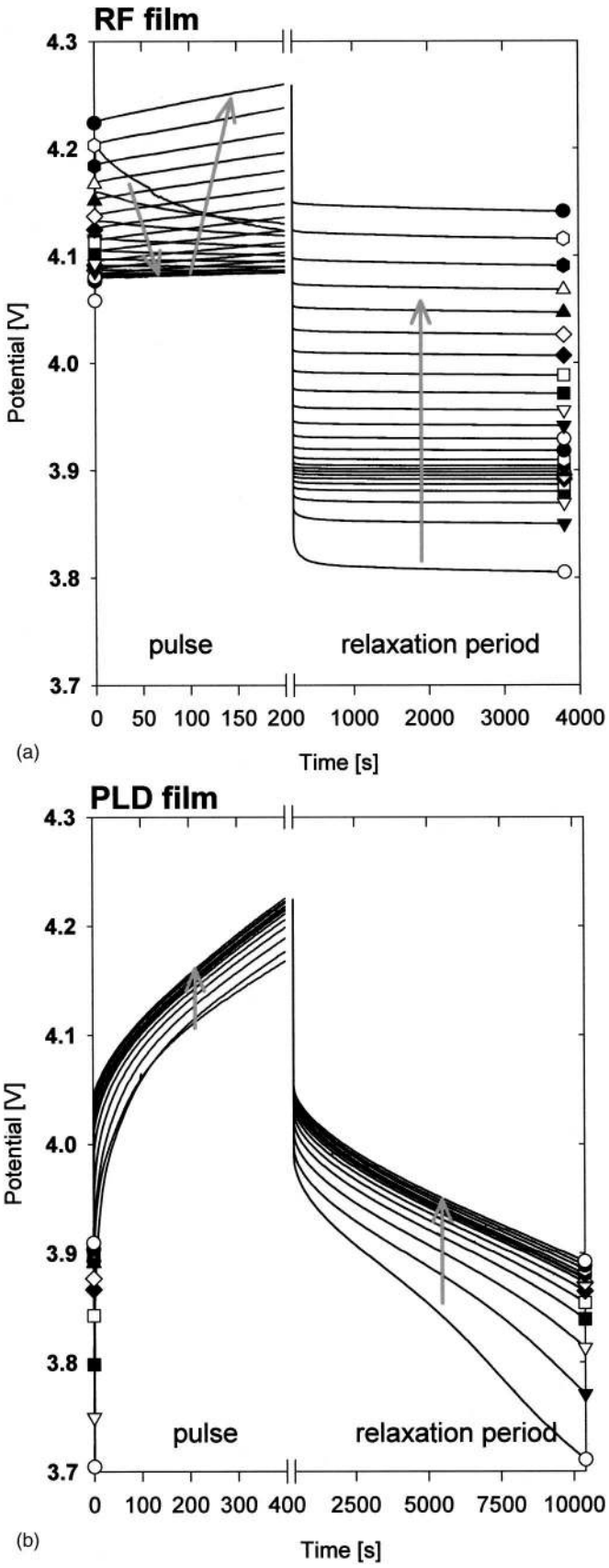

Figure 3. Potential response of the RF film (a) and the PLD film (b) to a positive current pulse of 10 μA/200 s and 1 μA/400 s, respectively. Both the pulse width and the subsequent zero current relaxation period are shown. The markers indicate the beginning and end of each curve and the arrows indicate their sequence.

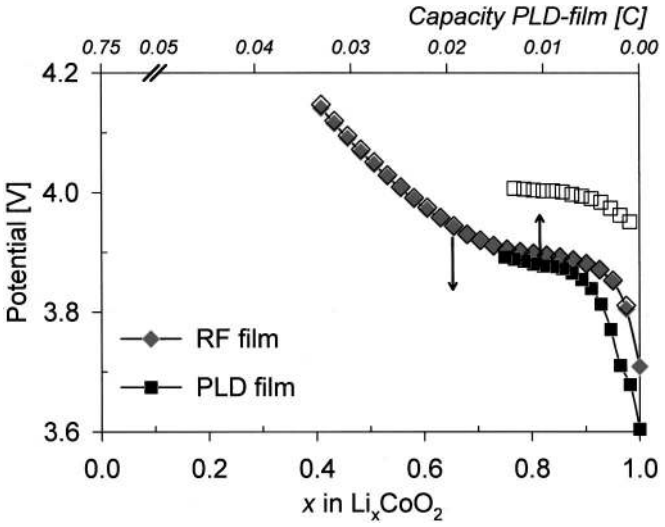

Figure 4. OCP of the RF film (◇) and the PLD film (□) as a function of the degree of lithium intercalation. The open markers (◇ and □, respectively) indicate the calculated E^{eq} for both films. The top axis, scaling the PLD film capacity, is stretched to match the potential curve of the RF film (see text).

$$\frac{d(OCP)}{dt} = \frac{d(OCP)}{dQ}\frac{dQ}{dt} \equiv \frac{d(E^{eq})}{dQ} i_{leakage} = \dot{E}^{decay} \qquad [2]$$

where Q stands for the stored charge in coulombs. The apparent leakage current $i_{leakage}$ is plotted in Fig. 5b for the RF and PLD film. In case of the RF film the current is approximately 0.04 μA up to 4 V and then shows a linear increase to 0.06 μA at 4.15 V. Since little charge is lost during relaxation, the x value of the RF film data in Fig. 4 needs no correction. The apparent leakage current of the PLD film shows a dramatic increase toward 10 μA above 4 V. At some point the leakage current fully consumes the intercalated charge during the open-circuit relaxation period and no higher OCP can be attained using pulsed charging with this specific pulse width/relaxation time rate. Note that the capacity values of the PLD film curve in Fig. 4 have not been corrected for this current leakage, as the large error would make an estimation of the actual lithium content highly unreliable.

In Fig. 6 the cell potential is plotted as a function of the relative extracted capacity (also called state of charge), (SOC) during galvanostatic cycling of the RF and PLD films *vs.* lithium using different current loads. The lower cutoff voltage is set at 3.0 V for both films. The upper cutoff voltage is set at 4.3 V for the RF film and 4.5 V for the PLD film, as this film shows significantly higher overpotentials at the same current density. At equal current densities, related to the macroscopic surface area, the RF films are able to supply a larger percentage of their theoretical capacity than the PLD films do between the limits of their cutoff voltage specifications. The capacity retention of the RF films is even maintained under larger loads. Due to the competitive effect of the apparent leakage current, very low charge and discharge currents do not enhance the reversible capacity of PLD films. The irreversible capacity, Q_{irr}, is indicated for the 0.5 μA curve at the bottom of the PLD film graph.

To obtain complementary data on the underlying intercalation mechanism, potential steps have also been applied to change the equilibrium composition of the electrode. The subsequent electric current may be analyzed according to the potentiostatic intermittent titration technique (PITT) to evaluate a chemical diffusion coefficient.[10] The potential of the cell is increased in steps of 50 mV from 3.80 to 4.20 V, while the current is measured with a sampling rate of 100 Hz for the first second, 10 Hz for the next 10 s and at 1 Hz for the next hour. Both films show an extremely fast current decay in the first 0.05 s (10^{-3} to 10^{-5} A). This part is disregarded in the graph as well as in the discussion, as it is assumed to be a capacitive artifact induced by the measurement equipment. The subsequent part of the current response is generally an order of magnitude larger for the RF film than for the PLD film (approximately 1-9 μA *vs.* 0.1-0.3 μA, respectively), although the residual current at the end of the relaxation period is generally larger for the PLD film. Figure 7 shows the current relaxation of the 0.75 μm RF film in a two-electrode setup. It is remarkable that after stepping the potential to 4.00 V the resulting current remains constant for almost an hour. In the plateau region of the OCP profile the intercalation process appears rate limited by a kinetic process other than single-phase diffusion. The next potential step to 4.05 V shows an increase in current density and with the following steps the trend of exponential-like current decay is regained. The PLD film shows exponential current decay at all potential steps.

Figure 8 shows the Nyquist plot of an RF film recorded at several SOC in the frequency range 10^5 to 10^{-2} Hz. The impedance of the lithium counter electrode proved insignificant in a lithium-lithium test configuration. Hence, it is assumed that the lithium electrode does not contribute to the overall impedance. The initial spectrum recorded directly after cell construction (open circles) is transformed with the cycling of the cell. The impedance spectrum of the cycled RF film resembles the cycled PLD film spectrum, although in the latter case the absolute values for Z' and Z'' are an order of magnitude larger. Both spectra show a decrease in the impedance with charging of the cell (deintercalation of lithium). In the discussion one model is proposed, describing both types of electrodes. In Fig. 13 the parameters of this equivalent circuit are plotted as function of OCP for a 0.50 μm RF film.

Phase transformations are known to occur for Li_xCoO_2 powders in the range $1 < x < 0.45$.[11] To investigate structural changes in these thin films, the temperature of the electrochemical cell is controlled accurately between 10 and 40°C at a specific SOC. It is assumed that the moderate temperature cycling itself does not induce phase transformation nor inflicts damage to the cell. The measured OCP(x) is plotted in Fig. 9a as a function of absolute temperature. It is related to the Gibbs free energy $G(x)$ as follows

Table I. Parameters of empirical Eq. 1 and 2 describing the potential relaxation of the RF and PLD film electrodes during pulsed current charging. The data sets are listed according to the amount of intercalated charge.

	Capacity (C)	E^{eq} (V)	a (V)	τ_a (s^{-1})	b (V)	τ_b (s^{-1})	i_{leak} (A)
RF film	0.01	3.811	9.2×10^3	50	1.7×10^2	334	3.1×10^7
	0.06	3.892	1.6×10^3	50	9.5×10^4	632	4.5×10^7
	0.12	3.920	8.9×10^4	60	1.8×10^3	554	4.4×10^7
	0.18	4.009	2.1×10^3	53	9.6×10^4	1057	4.1×10^7
	0.24	4.147	2.0×10^3	48	1.8×10^3	767	6.0×10^7
PLD film	0.001	3.951	8.7×10^3	63	2.6×10^2	577	1.4×10^6
	0.006	3.994	1.0×10^3	143	3.0×10^2	1388	3.0×10^6
	0.012	4.006	9.8×10^3	150	3.3×10^2	1640	9.5×10^6

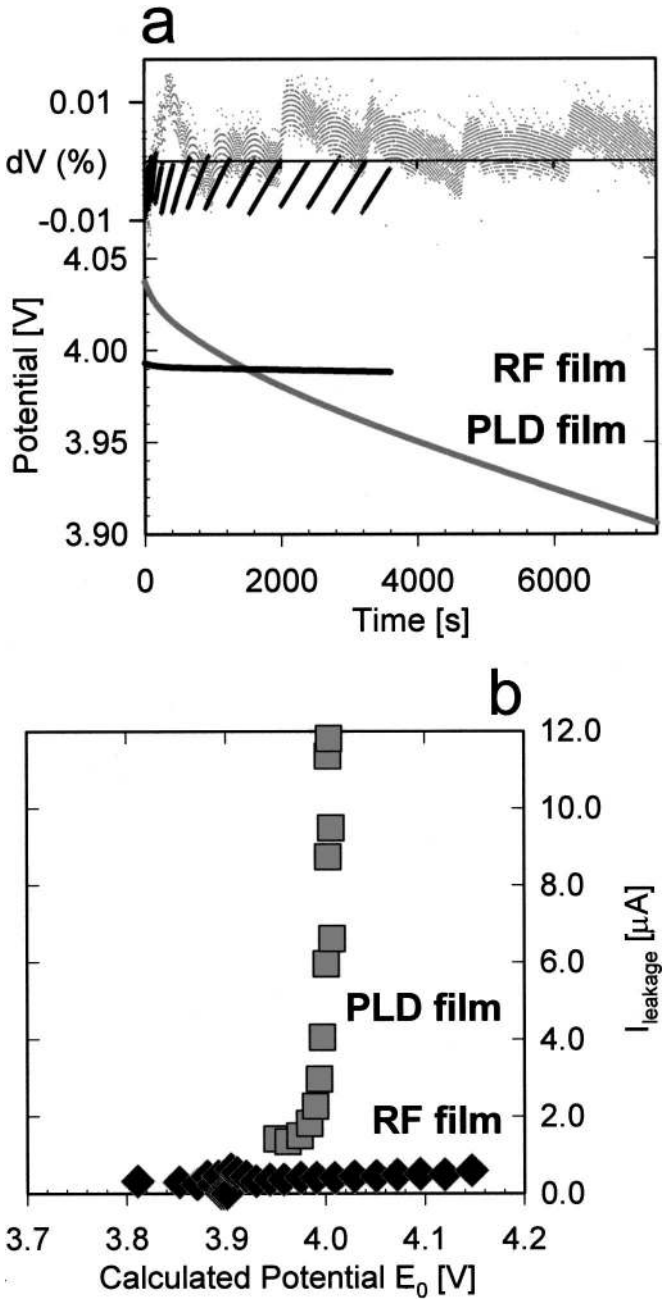

Figure 5. (a) Shows the potential relaxation of both film types according to Eq. 1. The inset graph shows the relative deviation between the raw data and the fit. (b) The apparent leakage current i_{leakage} is plotted for the RF film (♦) and the PLD film (□) as a function of potential.

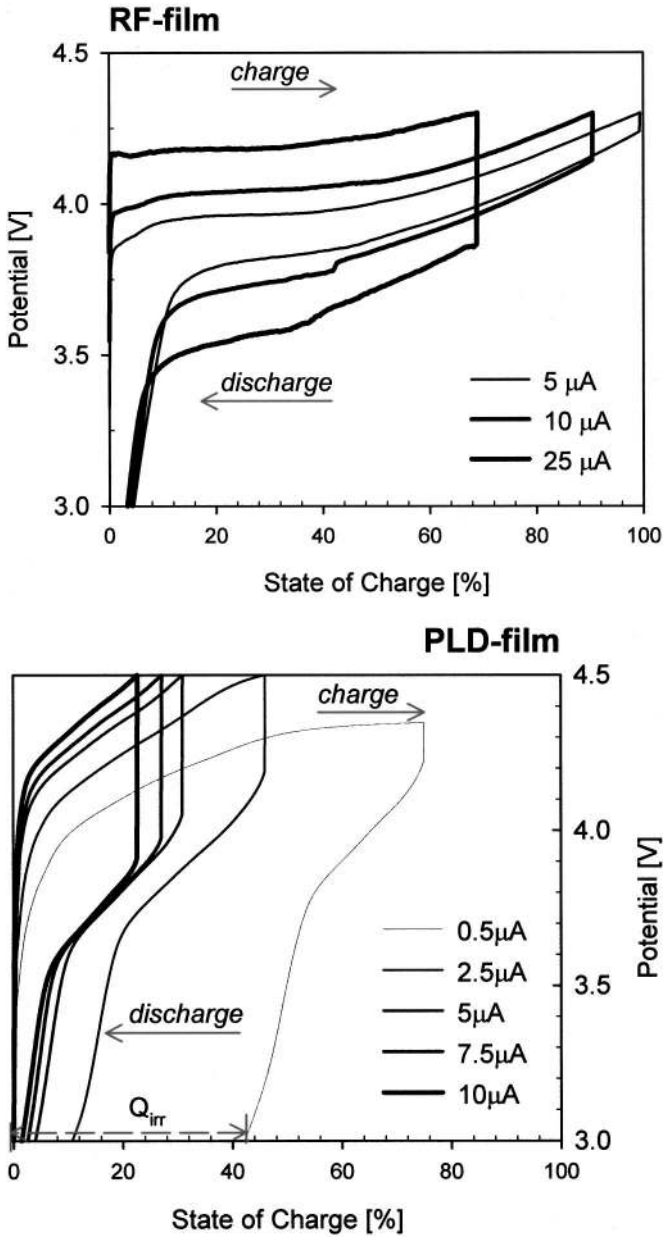

Figure 6. Constant current charge and discharge of the RF film (top) and the PLD film (bottom) plotted as function of SOC. Note that the charging currents of the RF film are larger than those applied to the PLD film.

$$\Delta G(x,T) = -nF \cdot OCP(x,T) \quad [3]$$

$$dG(x,T) = \sum_i \mu_i dx_i = (\mu_{\text{Li}}^{\text{Li}} - \mu_{\text{Li}}^{\text{Li}_x\text{CoO}_2})dx = -nFdOCP(x,T) \quad [4]$$

The chemical potential of lithium (μ_{Li}) in either electrode is defined by its partial molar entropy (s_{Li}) and partial molar enthalpy (h_{Li}). Both contributions are derived from the temperature dependence of the open cell potential using the modified Gibbs-Helmholtz equation with

$$\mu_{\text{Li}} = h_{\text{Li}} - Ts_{\text{Li}}$$

$$s_{\text{Li}}^{\text{Li}_x\text{CoCO}_2} - s_{\text{Li}}^{\text{Li}} = \left(\frac{\partial S}{\partial x}\right)_T = -\left(\frac{\partial G}{\partial T}\right)_x = -\frac{1}{nF}\left(\frac{\partial OCP}{\partial T}\right)_x \quad [5]$$

$$h_{\text{Li}}^{\text{Li}} - h_{\text{Li}}^{\text{Li}_x\text{CoO}_2} = \left(\frac{\partial H}{\partial x}\right)_T = \left\{\frac{\partial[G(x)/T]}{\partial(1/T)}\right\}_x = \frac{1}{nF}\left(\frac{\partial(OCP(x)/T)}{\partial(1/T)}\right)_x \quad [6]$$

The results for the RF film are plotted in Fig. 9b, where the partial molar enthalpy (gray squares) is scaled on the left and the partial molar entropy (open circles) is scaled on the right. The slope of both curves changes simultaneously, suggesting that a phase transformation occurs at those specific compositions (vertical dotted lines drawn as a guide to the eye). The inset reveals a phase diagram reported by Dahn *et al.*[12] No discrepancy is observed between ex-

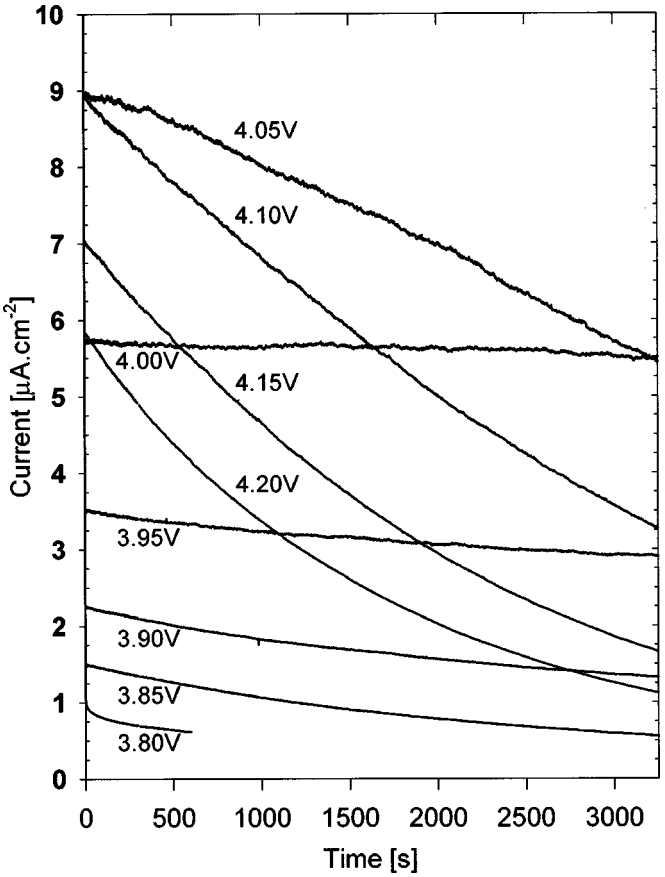

Figure 7. Current response of a 0.75 μm RF film to sequential 50 mV potential steps from 3.80 to 4.20 V as function of time.

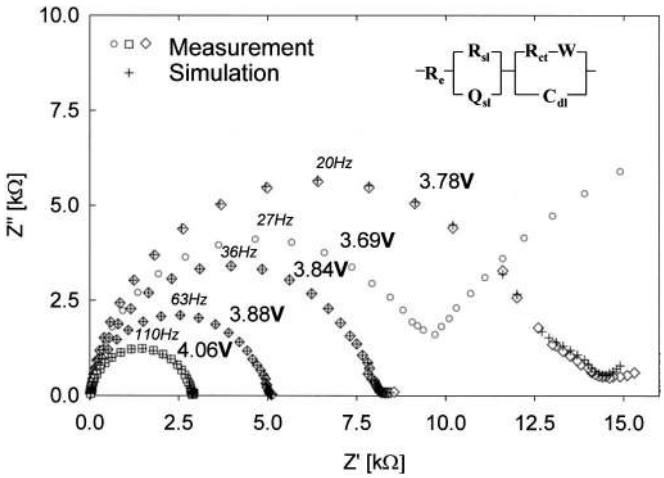

Figure 8. Nyquist plot of the RF film impedance directly after cell construction (○), in charged state (□), and at intermediate SOC (◇). Simulated responses, according to the inset equivalent circuit, are presented by (+). The *OCP* of the measurement and the summit frequency of the semicircles are indicated.

periments performed with increasing or decreasing SOC. This indicates a lack of hysteresis and a good reproducibility of the measurement results.

After electrochemical characterization the electrode is disconnected and analyzed with atomic force microscopy (AFM) and X-ray diffraction (XRD) to assess cycling-induced changes. Figure 10 shows the XRD spectrum of an RF film in discharged state ($x \approx 1$), recorded before and after extensive electrochemical cycling. For this analysis the sample has been tilted a few degrees to suppress the monocrystalline silicon diffraction peaks. The baseline intensity of the before situation has been vertically displaced for clarity. Besides the increase of the baseline noise, a slight increase of the Co_3O_4 content is observed. The preferential orientation of the host lattice is preserved.

The surface of the RF film is visualized in Fig. 11 using AFM tapping mode. The left AFM image Fig. 11a shows the electrode surface before electrochemical cycling, and the right image (Fig. 11b) shows the situation afterward. In order to clearly show the surface structure and roughness, the shading is greatly exaggerated. The impression is given that during electrochemical cycling an additional surface layer covers up the original microstructure. Image analysis reveals that the actual surface area of the RF film decreases from 152% before cycling to 122% after cycling, relative to the geometric surface area of 0.16 μm^2. The PLD films show a decrease from 119 to 108%. The difference is directly related to the surface roughness of the samples, which is largest for the RF films. Further specifications are listed in Table II.

Discussion

Both $LiCoO_2$ films show electrochemical lithium deintercalation activity as the positive electrode in a lithium/EC:DEC-$LiClO_4$ (1 M)/$LiCoO_2$ cell. The thin film performance depends heavily on the preferential orientation of the intercalation host structure. For example, almost the full theoretical capacity can be extracted from the RF film with 100% faradic yield using cyclic voltammetry at a scan rate of 0.1 mV s^{-1}, while at this rate the PLD film releases merely 0.1% of its theoretical capacity with a yield of only 6%. The absence of a distinct anodic peak is attributed to a high overpotential during cycling, which lowers the cathodic peak to potentials 0.2 V below the measured OCP plateau (Fig. 4) and the anodic peak is shifted above the cutoff potential.

The strong dependence on the host lattice orientation is caused by the exposure of the lithium diffusion planes toward the electrolyte solution. Theoretically, the RF film is fully open for intercalation. Hence, the entire film is directly involved in the intercalation process and, due to the fast inward diffusion of lithium, equilibration is quickly achieved. The diffusion planes in the PLD film are closed off and accessible only through openings provided by film irregularities and surface roughness.

As has been reported also by Iriyama *et al.*[5] only material in close proximity to these defects can contribute to the intercalation process. The intercalation rate and capacity of our PLD films have indeed been observed to improve with the etching of a gauze-like pattern into the existing PLD film or the application of stainless steel substrates.[6]

Figure 12 shows a schematic representation of the intercalation process in Li_xCoO_2 in the case of RF (a) and PLD films (b), where CT stands for charge transfer, $I_{leakage}$ the leakage current due to electrolyte decomposition, $D_{\parallel}$ the in-plane lithium diffusion, $D_{\perp}$ the slow cross plane lithium diffusion, and Tr indicates the direction of host-phase transformation. These elements are addressed and correlated to the observed phenomena in the following discussion.

Leakage current.—As the intercalation into the PLD film is restricted to the surface region of the Li-CoO_2, relatively little charge can induce a potential far from the equilibrium value of the electrode. Evidence is the high overpotentials and the low (reversible) capacity observed with galvanostatic cycling. A high surface potential of the intercalation electrode will also accelerate the oxidation of the electrolyte (and simultaneous electrode reduction), causing increased self-discharge and irreversible capacity loss. The apparent leakage current, estimated from pulsed current charging (galvanostatic intermittent titration technique, GITT), is indeed particularly strong above 4 V (Fig. 5b).

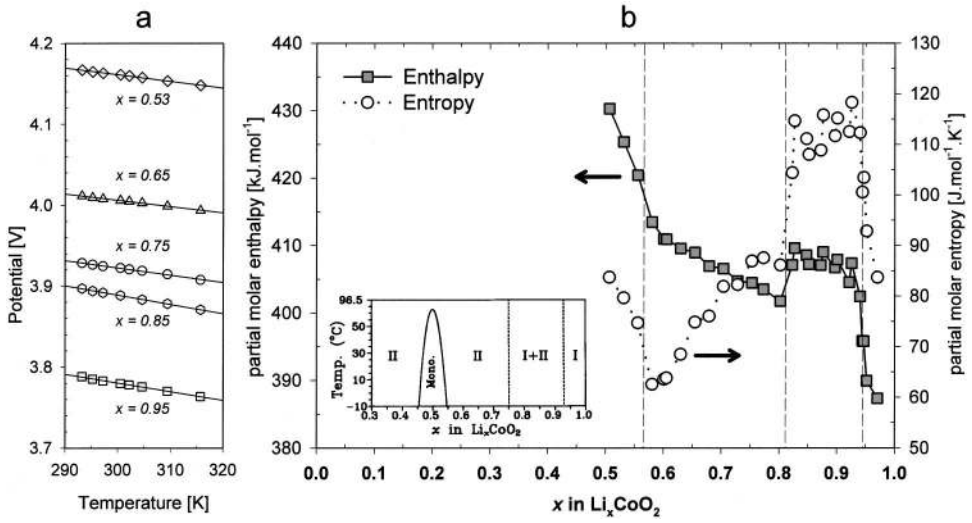

Figure 9. (a) Shows the measured OCP of a 0.75 μm RF film as a function of temperature at the specified SOC and (b) shows the calculated partial molar enthalpy (■) and entropy (○) as functions of the lithium composition. Both curves change at similar lithium concentrations corresponding to the inset phase diagram reported by Reimers and Dahn.[12]

The mechanism of the electrolyte decomposition is expected to be similar for RF and PLD films. As the RF film also exhibits the largest surface area, the large difference in the apparent leakage current is unexpected. The residual currents measured with potentiostatic intermittent titration technique (PITT) can be interpreted as the actual leakage current and show a similar trend as the apparent leakage current shown in Fig. 5b. The actual leakage current increases from 0.05 μA at 3.9 V to 0.18 μA at 4.20 V for the PLD film and exceeds the residual current values of the RF film by a factor two, which is more plausible. Comparable currents are recorded with cyclic voltammetry to maintain a steady cell potential. The difference between the apparent and actual leakage current of the PLD film indicates that the linear part of the potential decay under open-circuit conditions cannot be attributed solely to electrolyte decomposition.

Lithium diffusion.—The intercalated charge at the surface of the electrode is equilibrated through inward diffusion of the lithium concentration gradient. If this intercalation process is diffusion-limited we can assume semi-infinite conditions for short times ($t \ll L^2/\tilde{D}$) and define an effective diffusion coefficient from the pulsed current charging experiment according to the GITT[10]

$$\frac{dE}{dt^{1/2}} = V_m \frac{dE}{dx} \frac{2I}{zFS(\pi\tilde{D})^{1/2}} \qquad [7]$$

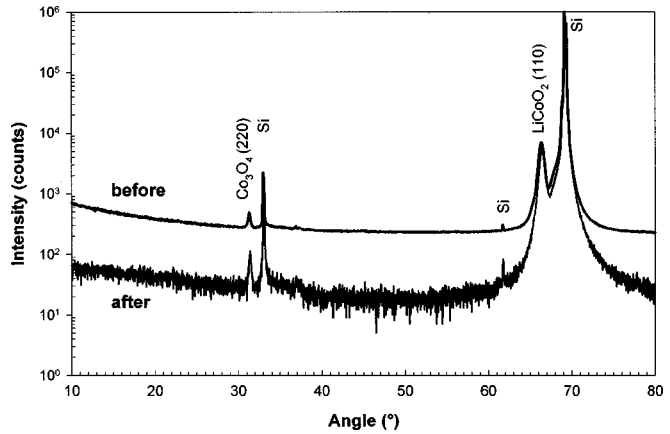

Figure 10. XRD spectra of the 0.75 μm RF film recorded before and after electrochemical analysis. The reflections of the silicon substrate are marked with Si.

where V_m is the molar volume, I is the pulse current, z the number of electrons ($z = 1$), F the faradaic constant, S the surface area, and $\tilde{D}$ the chemical diffusion coefficient. This equation does not provide a convincing fit for the experimental RF and PLD film data over extended time periods. Confining our data to the first 50 s yields an effective chemical diffusion coefficient of approximately 10^{-4} and 10^{-14} cm^2 s^{-1}, respectively (plotted in Fig. 13). The first value is orders of magnitude above chemical diffusion coefficients reported even for composite electrodes.[13] Based on this chemical diffusion coefficient the maximum measurement time would be $5 \cdot 10^{-5}$ s, which is an order of magnitude smaller than the 50 s used for the calculation. This discrepancy indicates, that the observed potential relaxation is not related to a true diffusion process and the diffusion coefficient calculated with this (or any other) semi-infinite diffusion model must be regarded as an effective one. The PLD film does reveal an effective chemical diffusion coefficient of the expected order of magnitude. Even though the extracted quantities are indicative, the absolute difference is remarkable and agrees with the strongly anisotropic lithium diffusion.

A diffusion coefficient can also be deduced from the current relaxation following a potential step according to the PITT.[10] The current response of the PLD film confirms the low diffusion coefficient value found previously with GITT, while the RF film response does not match this model; the current becomes virtually constant after stepping to 4.0 V (Fig. 7), suggesting a kinetically limited intercalation reaction. This potential lies just above the OCP(x) voltage plateau and corresponds to the end of the two-phase intercalation region. With this particular 50 mV step a large amount of lithium is deintercalated, which induces a phase transformation. Here the phase boundary movement is expected to be the rate-determining process, as the next potential step shows a further increase in the initial current response and subsequent decay.

Phase transformation.—Phase transformation of the RF films is revealed by resolving the OCP(T) at a specific SOC into a the temperature-dependent component (partial molar entropy difference) and temperature independent component (partial molar enthalpy difference) which both are plotted in Fig. 9b. The potential of the lithium counter electrode is assumed constant, and thus all features are attributed to the working electrode (in other words, s_{Li}^{Li} and h_{Li}^{Li} are assumed to be constant).

The changes in the partial molar entropy and enthalpy as functions of lithium concentration correspond well with the inset phase diagram in Fig. 9b. The absolute values of x could be slightly overestimated due to the slowly receding intercalation capacity (*e.g.*, $x = 0.55$ is in fact $x = 0.50$). Phase I and II denote two rhombohedral structures with different lithium concentrations and both exist in the

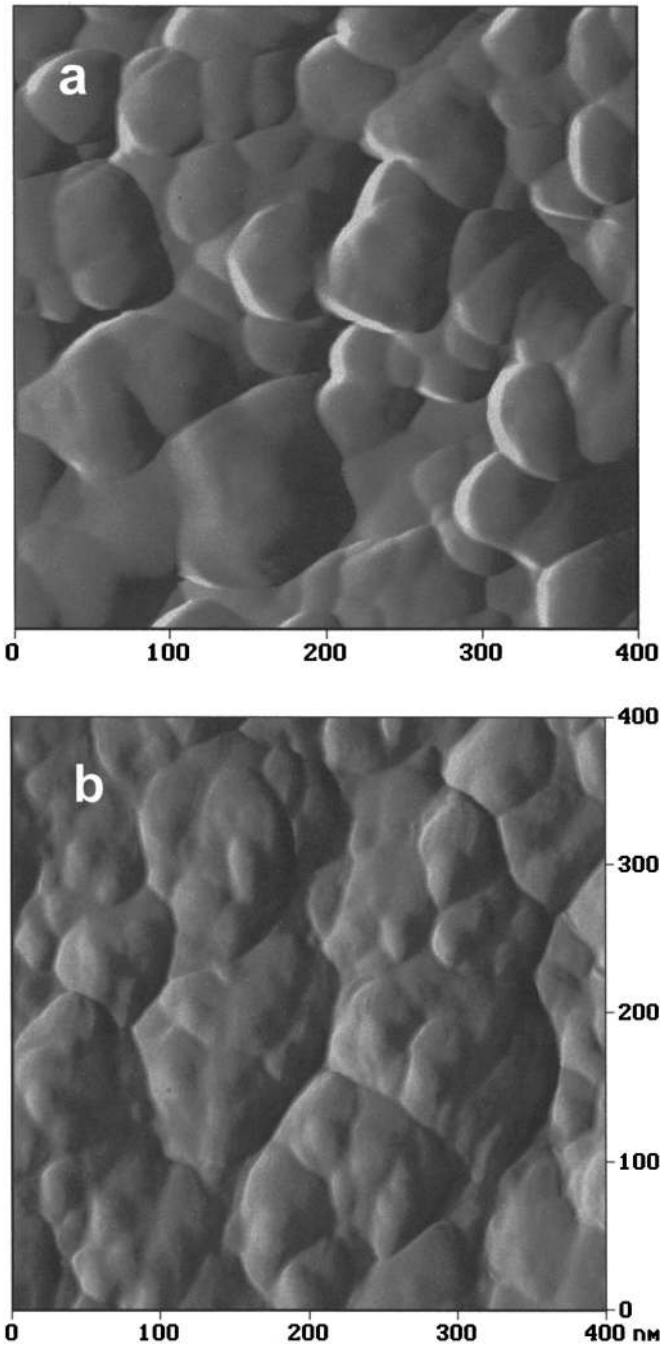

Figure 11. AFM amplitude plot of the 0.75 μm RF film obtained in tapping mode before exposure to electrolyte solution (a) and after extensive electrochemical cycling (b). Note the coloring does not represent absolute height.

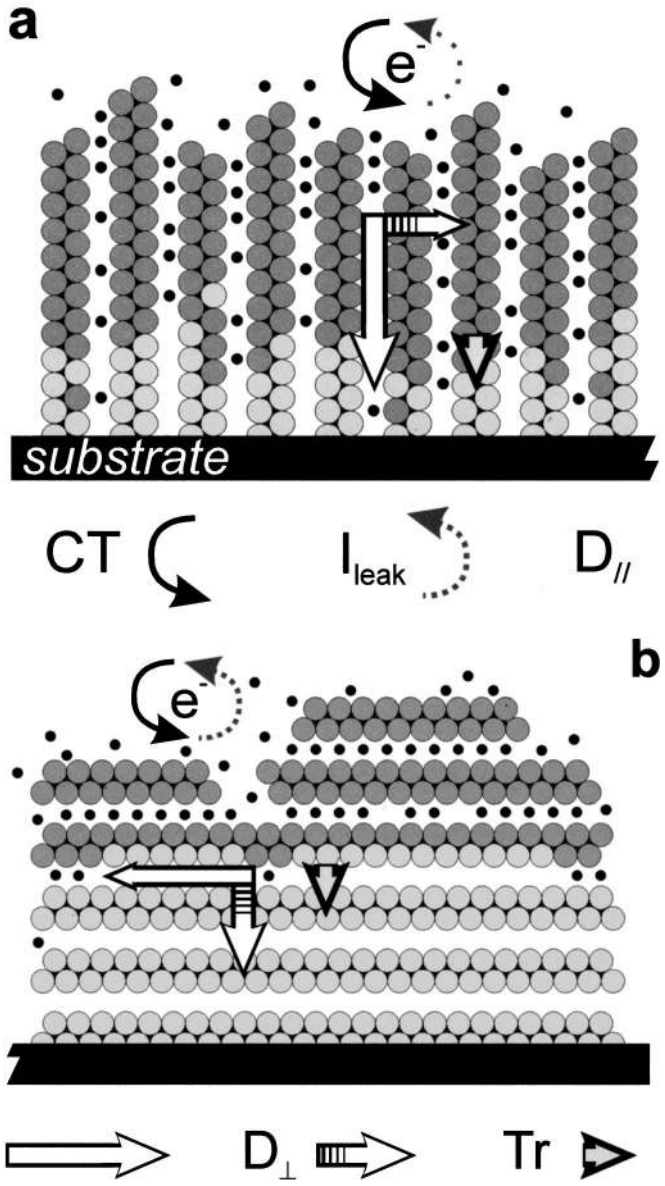

Figure 12. Schematic model representing the host structure of the RF film (a) and the PLD film (b). The arrows represent the direction of the processes involved in lithium intercalation and are denoted in the legend below the schematic: charge transfer (CT), current leakage ($I_{leakage}$), lithium diffusion parallel ($D_{\parallel}$), and perpendicular ($D_{\perp}$) to the diffusion planes and phase boundary movement (*Tr*).

Table II. Image analysis results calculated from AFM surface scans of RF and PLD film before and after electrochemical cycling in liquid electrolyte (EC:DEC 1:1, 1 M $LiClO_4$).

	RF film		PLD film	
	Before	After	Before	After
Z range (nm)	114.62	64.87	31.56	25.81
RMS roughness (nm)	17.36	10.66	5.63	4.35
Image surface area (μm^2)	0.243	0.196	0.190	0.173
Image surface area difference	51.8%	22.3%	18.7%	7.9%

two-phase region in the range $0.75 < x < 0.93$. The left region specified as *Mono* indicates the monoclinic $Li_{0.5}CoO_2$ stability range and corresponds to composition $x < 0.57$. In the two-phase region the applied GITT and PITT diffusion equations are not applicable and thus only an effective diffusion coefficient, correlated to the phase boundary diffusion, is calculated in the range 3.87-3.93 V *vs.* lithium.

For $LiCoO_2$ powders the phase transformation from phase I to II is accompanied with a *c* axis increase (14.09 to 14.26 Å) and a small *a* axis decrease (2.816 to 2.812 Å) of the unit cell, resulting in a volumetric expansion of approximately 1%.[12] In case of the RF films the *c* axis lies parallel to the surface and might suffer some constraint due to the substrate confinement. However, no cracking or peeling of the 0.75 μm film is observed with cycling of the cell. During this process the preferential orientation of the host lattice is

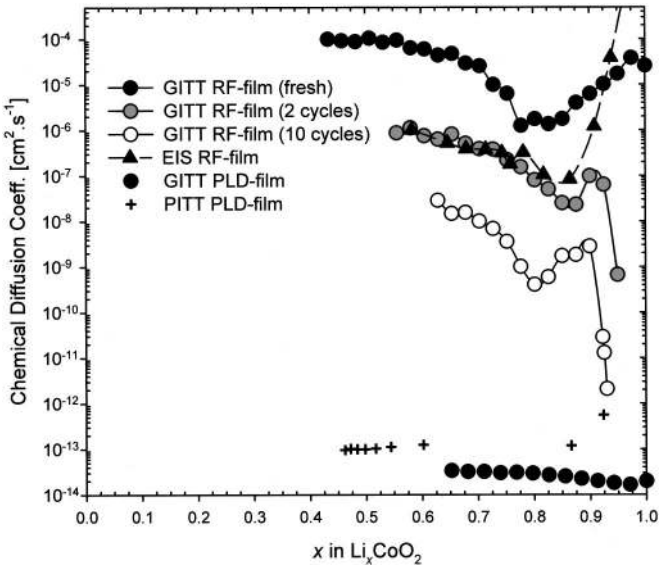

Figure 13. The apparent chemical diffusion coefficient calculated with GITT, PITT, and EIS for the RF and PLD film electrodes plotted as a function of x.

also maintained. Apparently, the phase transformation is well feasible, unhindered by the bonding to the substrate.

The partial molar entropy shows a strong increase upon lithium deintercalation from $LiCoO_2$, due to the introduction of lithium vacancies and electronic charge carriers. In the two-phase region the partial molar entropy and enthalpy are approximately stable, as the Gibbs free energy (sum of h_{Li} and Ts_{Li}) designates the plateau potential. Upon further lithium extraction the Li_xCoO_2 enters the single-phase region II and the partial molar enthalpy increases with the charging of the electrode, while the partial molar entropy decreases due to clustering of vacancies to the point where a long-range ordered structure remains.[14] Lithium deintercalation from this monoclinic phase leads to a strong increase in both partial molar enthalpy and entropy. No further deintercalation was attempted.

Phase transformation is also expected to occur in the PLD film, but it could not be analyzed as a function of temperature due to the unstable OCP. However, the estimated equilibrium potential E^{eq} obtained from pulsed charging, predicts that the PLD film electrode has initially a potential around 4 V, which coincides with the phase II region of the RF film. It is possible that with each charge pulse, phase transformation is induced at the surface of the PLD film electrode. Lattice expansion upon lithium deintercalation is unhindered by bonding to the substrate due to the c axis orientation. Lithium extraction from the exposed diffusion planes is expected to be as fast as observed for the RF films and results in a layer-by-layer deintercalation plus transformation of the host structure. The simultaneous phase boundary movement would restrain the (de-)intercalation process.[13]

Equivalent circuit.—Analysis of the intercalation process in the frequency domain is suitable for providing physical interpretation of the electrochemical behavior. The empirical Eq. 1 describing the time-dependent potential relaxation can be converted to the frequency domain using a Laplace transformation. However, the high frequency end (>1 Hz) of the Li-transformed data is rather inaccurate due to the sampling rate limitation. There are some analogies with the impedance spectra data such as the similarity in the relaxation time constants of the RF and PLD films is reflected by the mutual resemblance of the impedance spectra and the ratio of the pre-exponential factors corresponds to the tenfold higher impedance of the PLD films.

The model that describes the frequency-dependent behavior of both types of electrodes successfully is drawn as an equivalent circuit in the inset in Fig. 8. This basic model has been applied successfully for numerous intercalation materials.[15] R_e stands for the electrolyte resistance, R_{sl} and Q_{sl} represent the interface with a surface layer (signifies the SEI layer). The charge-transfer resistance, double-layer capacitance and diffusion are described with a Randles circuit using the elements R_{CT}, C_{dl}, and W, respectively. The equivalent circuit is fitted to the impedance spectra using Equivalent Circuit.[16] The pseudo χ^d value ranges from 10^{-4} to 10^{-6} indicating acceptable fits. Figure 12 shows the values of the equivalent circuit parameters for a 0.5 μm RF film as a function of potential *vs.* lithium in 10 mV steps. The electrolyte resistance is not presented, since it remains constant at 17 Ω.

The dominant semicircle in the Nyquist plot of the RF (Fig. 8) and the PLD film scales inversely with increasing SOC and is associated with the $R_{CT}C_{dl}$ network. The summit frequency changes from 20 to 110 Hz for RF film and from 0.5 to 0.8 Hz for PLD film. The double-layer capacity, assumed equal to the constant phase element, Q_{dl}, as n_{dl} approximates unity, appears almost equal for the RF film and the PLD film ($0.9 \cdot 10^{-6}$ and $1.4 \cdot 10^{-6}$ F, respectively) indicating a similar contact with the electrolyte. The Q_{dl} for the PLD film remains constant at all SOC, but the RF film value shows a decrease at 3.72 and 3.88 V suggesting a correlation to the phase transformation I → I + II → II. The small variations in the n value of the constant phase element show a similar, but inversed trend.

The charge transfer resistance R_{CT} is related to the exchange current density, i_0, by the equation

$$i_0 = \frac{RT}{zFR_{CT}} \quad [8]$$

In the discharged state the charge-transfer resistance is high, but it decreases rapidly and stabilizes at 3.90 V. Levi *et al.*[17] reported similar behavior for porous $LiCoO_2$ electrodes. The calculated exchange current density of the 0.50 μm RF film is initially 10^{-5} A cm^{-2} and increases to $3 \cdot 10^{-5}$ A cm^{-2}. Again the trend seems to follow the phase transformations, as observed above with Q_{dl}. In the case of the PLD film the exchange current density shows a slight increase from 10^{-7} to $1.7 \cdot 10^{-7}$ A cm^{-2} at 4.14 V. Although the PLD film kinetics are clearly inferior, the charge-transfer resistance of both films is high compared to composite electrodes and is responsible for the high overpotentials.

After subtraction of the charge-transfer related semicircle from the Nyquist plot, a smaller semicircle with lower summit frequency remains, which can be described by the surface layer network consisting of a parallel resistance R_{sl} and the constant phase element Q_{sl}. The impedance of these elements also appears dependent on the cell potential and increases gradually with aging of the sample. Lithium deintercalation from stoichiometric $LiCoO_2$ causes an immediate decrease of R_{sl} and a simultaneous response of Q_{sl}; both stabilize beyond 3.75 V. This trend appears related to the increase in electronic conductivity as the $LiCoO_2$ changes from semiconducting to conducting. In case of the PLD film the impedance characteristics of the surface film are small compared to the large influence of R_{CT} and could not be resolved accurately.

The Warburg coefficient in Fig. 14 also shows a strong phase dependency. It remains stable at low potentials and shows a steady increase toward the maximum obtained at the plateau potential at 3.9 V. This peak corresponds to a minimum in the chemical diffusion coefficient (see Eq. 9), which is expected in a two-phase region and confirmed by the measurements in time domain. The linear decrease in the Warburg coefficient upon further charging suggests that

[d] The modulus weighted, mean variance between experimental data and fit.[16]

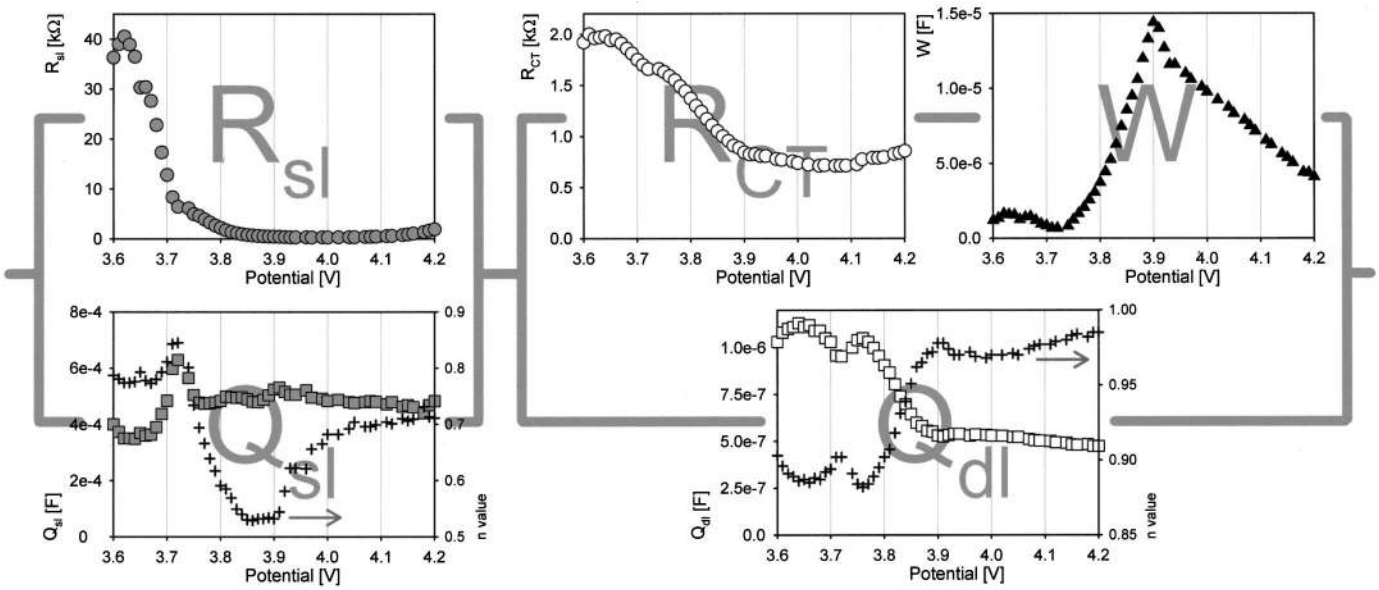

Figure 14. The values of the equivalent circuit parameters used to fit the impedance spectra of a 0.50 μm RF film plotted as function of potential.

the diffusion rate increases with increasing lithium deficiency in the single-phase II region.

Assuming semi-infinite conditions, the chemical diffusion coefficient of the RF film can be estimated from the Warburg impedance Z_W [10]

$$Z_W = \frac{V_M}{\sqrt{2}zFA\tilde{D}_{Li}^{1/2}}\frac{dE}{dx}(1 - j)\omega^{-1/2} = W(1 - j)\omega^{-1/2} \quad [9]$$

where W is the Warburg coefficient, V_M the molar volume of the host structure, dE/dx the slope of the $OCP(x)$ plot, z the number of the electrons involved in the charge-transfer ($z = 1$), and ω the radial frequency. The chemical diffusion coefficient calculated for the 0.75 μm RF film is plotted together with the other corresponding semi-infinite diffusion coefficient estimates in Fig. 14. The Warburg impedance indicates high chemical diffusion coefficients. These show good similarity to the values calculated from the second GITT experiment, which was performed just before the impedance measurement. The upward deviation, observed as x approaches unity, is the result of fitting inaccuracy in the low frequency domain. As there is no evidence of a transition of semi-infinite to finite space diffusion at a specific frequency, the value calculated with Eq. 9 from the Warburg impedance must also be regarded as an effective chemical diffusion coefficient for the lithium (de-)intercalation process.

The outstanding performance of the RF film is subject to deterioration. The GITT estimate of the chemical diffusion coefficient after ten cycles clearly shows a decrease in intercalation rate and capacity, but the shape of the curve remains the same. This suggests that the host material itself does not degrade upon cycling, but merely that less material is involved in the intercalation process. Due to the continuous increase of the surface film impedance, the aging effect is mainly attributed to the growth of a SEI layer on the electrode surface caused by electrolyte decomposition.[18] Avoiding contact with liquid electrolyte by applying a (thin) solid-state electrolyte layer could be the key to controlling the SEI and thus minimizing the capacity fade, provided that a passivation film with constant low charge-transfer resistance could possibly even enhance the current rate capability.

Conclusions

Thin film electrodes of $LiCoO_2$ have been prepared using RF sputtering and pulsed laser deposition and exhibit a perpendicular (hence accessible) and a parallel (thus inaccessible) alignment of the lithium diffusion plane towards the electrolyte solution, respectively. In the first case the full film capacity is involved, while in the second case only the surface of the electrode contributes to the electrochemical intercalation process and low capacities are observed. The favorable orientation of the RF films enables fast inward diffusion and thus a quick response to current pulses. The lithium intercalation process in PLD films is difficult and the potential relaxation slow. The apparent chemical diffusion coefficient estimated for the RF films is many orders of magnitude larger than that of the PLD film. Solid-state diffusion is not necessarily the rate-limiting process.

Phase transformation of the $LiCoO_2$ thin film electrode is observed at specific lithium concentrations and appears unhindered by the bonding to the substrate. These structural transformations affect the electrochemical characteristics of the intercalation electrode. The intercalation process is generally restrained by the large charge-transfer resistance and in some cases by phase boundary movement. Cycling does not lead to reorientation or permanent transformation of the host structure. The observed deterioration of intercalation rate and capacity is attributed to the growth of a SEI layer, which decreases the electrode surface area and poses an additional barrier for lithium intercalation.

For two-dimensional intercalation materials the accessible alignment of the lithium diffusion planes is essential for optimal electrode performance.

Acknowledgments

The authors are indebted to Philips Research Laboratory for all technical support in sample preparation and characterization and FOM for financial support. Special thanks are due to J. F. M. Cillessen for operation and assistance on the PLD equipment, L. H. G. J. Segeren for the AFM measurements, and the Philips CFT department for the XRD measurements.

The University of Twente assisted in meeting the publication costs of this article.

References

1. H. J. Bergveld, Ph.D. Thesis, p. 156, University of Twente, The Netherlands (2001).
2. A. van der Ven and G. Ceder, *Electrochem. Solid-State Lett.*, **3**, 301 (2000).
3. P. J. Bouwman, B. A. Boukamp, H. J. M. Bouwmeester, H. J. Wondergem, and P. H. L. Notten, *J. Electrochem. Soc.*, **148**, A311 (2001).
4. J. B. Bates, N. J. Dudney, B. J. Neudecker, F. X. Hart, H. P. Jun, and S. A. Hackney, *J. Electrochem. Soc.*, **147**, 59 (2000).

5. Y. Iriyama, M. Inaba, T. Abe, and Z. Ogumi, *J. Power Sources,* **94**, 175 (2001).
6. P. J. Bouwman, B. A. Boukamp, H. J. M. Bouwmeester, and P. H. L. Notten, in *Solid State Ionics Conference Proceedings*, 2001.
7. K. A. Striebel, C. Z. Deng, S. J. Wen, and E. J. Cairns, *J. Electrochem. Soc.,* **143**, 1821 (1996).
8. M. Antaya, J. R. Dahn, J. S. Preston, E. Rossen, and J. N. Reimers, *J. Electrochem. Soc.,* **140**, 575 (1993).
9. P. Fragnaud, T. Brousse, and D. M. Sleich, *J. Power Sources,* **63**, 187 (1996).
10. H. J. M. Bouwmeester and A. J. Burggraaf, in *CRC Handbook of Solid State Electrochemistry*, P. J. Gellings and H. J. M. Bouwmeester, Editors, CRC Press, Boca Raton, FL (1997).
11. X. Q. Yang, X. Sun, and J. McBreen, *Electrochem. Commun.,* **2**, 100 (2000).
12. J. N. Reimers and J. Dahn, *J. Electrochem. Soc.,* **139**, 2091 (1992).
13. Y. Jang, B. J. Neudecker, and N. J. Dudney, *Electrochem. Solid-State Lett.,* **4**, A74 (2001).
14. G. Ceder and A. van der Ven, *Electrochim. Acta,* **45**, 131 (1999).
15. M. Mohamedi, D. Takahashi, T. Uchiyama, T. Itoh, M. Nishizawa, and I. Uchida, *J. Power Sources,* **93**, 93 (2001).
16. B. A. Boukamp, *J. Electrochem. Soc.,* **142**, 1883 (1995).
17. M. D. Levi, G. Salitra, B. Markovsky, H. Teller, D. Aurbach, U. Heider, and L. Heider, *J. Electrochem. Soc.,* **146**, 1279 (1999).
18. D. Aurbach, *J. Power Sources,* **81-82**, 95 (1999).